Int J Thermophys (2010) 31:2275–2282
DOI 10.1007/s10765-010-0854-1

Combined FPPE–PTR Calorimetry Involving TWRC Technique. Theory and Mathematical Simulations

Dorin Dadarlat · Mircea Nicolae Pop · Mihaela Streza · Stephane Longuemart · Michael Depriester · Abdelhak Hadj Sahraoui · Viorica Simon

Received: 23 April 2010 / Accepted: 8 October 2010 / Published online: 30 October 2010

Abstract Photopyroelectric calorimetry in the front detection configuration (FPPE) was combined with photothermal radiometry (PTR), in order to investigate dynamic thermal parameters of different layers of a detection cell. The layout of the detection cell consists of three layers: directly irradiated pyroelectric sensor, liquid layer, and solid backing material; and the scanning parameter is the thickness of the liquid layer (thermal-wave resonator cavity method). The theory developed for the two techniques indicates that both FPPE and PTR signals can lead, in the thermally thin regime for the sensor and liquid layer, to the direct measurement of the thermal diffusivity or effusivity of the sensor and/or liquid layer, or the thermal effusivity of the backing material. The two methods offer complementary results and/or reciprocally support each other.

Keywords PPE calorimetry · PTR radiometry · Thermal parameters · TWRC method

D. Dadarlat · M. N. Pop · M. Streza (✉)
National R&D Institute for Isotopic and Molecular Technologies, Donath Str. 65-103, 400293 Cluj-Napoca, Romania
e-mail: streza.mihaela@gmail.com

S. Longuemart · M. Depriester · A. Hadj Sahraoui
Univ Lille Nord de France, CP 59000 Lille, ULCO, UDSMM, 59140 Dunkerque, France

V. Simon
Faculty of Physics, Babes-Bolyai University, 400084 Cluj-Napoca, Romania

1 Introduction

In the front photopyroelectric (FPPE) configuration, the radiation impinges on the front surface of the pyroelectric sensor, and the sample, in good thermal contact with its rear side, acts as a heat sink. In principle, an FPPE detection cell contains three layers: directly irradiated sensor, solid or liquid sample, and a semi-infinite backing material. The value of the dynamic thermal parameters (thermal diffusivity, effusivity, or conductivity) of the layers (sensor, sample, or backing) of the detection cell could be obtained by performing frequency or thickness (in the case of liquid samples) scans of the amplitude or phase of the FPPE signal. The thickness scanning procedure is associated with the so-called thermal-wave resonator cavity (TWRC) method, introduced about 10 years ago by Mandelis and co-workers and developed later by others groups [1–8]. The TWRC method, in the back detection configuration (BPPE), has been shown to be suitable and very accurate for investigating thermal properties (especially thermal diffusivity) of liquids [2,9,10].

Recently, we proposed a combined FPPE–TWRC method with the purpose of measuring the thermal effusivity of a solid material (inserted as backing in the detection cell) [11–14]. The main advantage of this configuration is connected with the possibility of monitoring the properties (type and thickness) of the coupling fluid, in order to obtain the thermal effusivity of a solid.

Concerning the PTR technique, it was largely used in the past, together with the frequency scan method, for calorimetric investigations of solid samples [15–20]. In such type of investigations, the irradiated layer is a thermally thin and opaque solid, and the normalization of the PTR signal involves some known thermally thick backings.

In this article, we propose a theoretical study of new, combined FPPE–PTR calorimetry, which also involves the TWRC scanning procedure.

2 Theory

The layout of the detection configuration is presented in Fig. 1. The radiation is partially absorbed by the front, opaque electrode of the thermally thin pyroelectric sensor. Air and backing layers are considered semi-infinite. The heat propagation through the layered system is considered one-directional. In order to obtain the FPPE and PTR signals, one has to solve the classical thermal diffusion equations with the boundary conditions for temperature and flux continuity [1]. Finally, in order to obtain the PTR signal, we have to deduce the temperature at the front surface of the sensor, and for the FPPE signal, we have to integrate the temperature distribution over the sensor's thickness. Due to the fact that the algebra connected with the calculation of the temperature distribution in the layers of such a sandwich system was already largely described [21,22], we will present only the final steps of the calculations in the following.

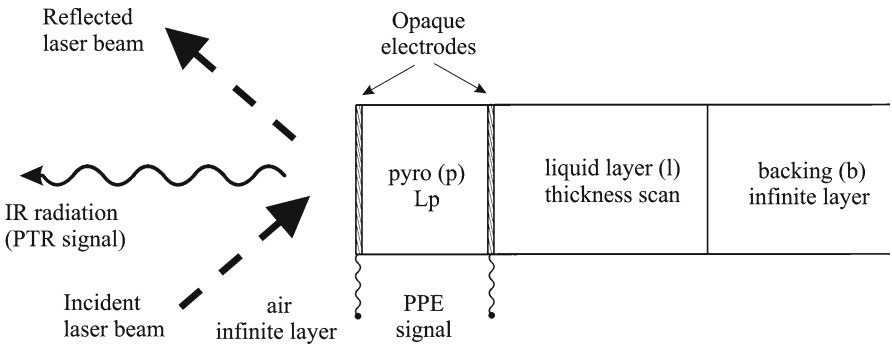

Fig. 1 Layout of the detection configuration

2.1 Front Photopyroelectric

In the approximation of one-directional heat propagation, the normalized complex PPE signal is given by [11]

$$V^{\mathrm{PPE}} = \frac{\left[S\left(b_{\mathrm{bl}}+1\right)\left(b_{\mathrm{lp}}+1\right)+S^{-1}\left(b_{\mathrm{bl}}-1\right)\left(b_{\mathrm{lp}}-1\right)\right](P-1)+\left[S\left(b_{\mathrm{bl}}+1\right)\left(b_{\mathrm{lp}}-1\right)+S^{-1}\left(b_{\mathrm{bl}}-1\right)\left(b_{\mathrm{lp}}+1\right)\right]\left(P^{-1}-1\right)}{\left[S\left(b_{\mathrm{bl}}+1\right)\left(b_{\mathrm{lp}}+1\right)+S^{-1}\left(b_{\mathrm{bl}}-1\right)\left(b_{\mathrm{lp}}-1\right)\right]P+\left[S\left(b_{\mathrm{bl}}+1\right)\left(b_{\mathrm{lp}}-1\right)+S^{-1}\left(b_{\mathrm{bl}}-1\right)\left(b_{\mathrm{lp}}+1\right)\right]P^{-1}} \tag{1}$$

where

$$S=\exp(\sigma_{\mathrm{l}}L_{\mathrm{l}}),\ P=\exp(\sigma_{\mathrm{p}}L_{\mathrm{p}}),\ \sigma_j=(1+\mathrm{i})a_j;\ \mu=(2\alpha/\omega)^{1/2},\ b_{ij}=e_i/e_j \tag{2}$$

In the thermally thin limit for the sensor, $\exp(\pm\sigma_{\mathrm{p}}L_{\mathrm{p}}) = 1 \pm \sigma_{\mathrm{p}}L_{\mathrm{p}}$, and Eq. 1 becomes

$$V^{\mathrm{PPE}}=\frac{\left[S\left(b_{\mathrm{bl}}+1\right)-S^{-1}\left(b_{\mathrm{bl}}-1\right)\right]\left(\sigma_{\mathrm{p}}L_{\mathrm{p}}\right)}{\left(\sigma_{\mathrm{p}}L_{\mathrm{p}}\right)\left[S\left(b_{\mathrm{bl}}+1\right)-S^{-1}\left(b_{\mathrm{bl}}-1\right)\right]+b_{\mathrm{lp}}\left[S\left(b_{\mathrm{bl}}+1\right)+S^{-1}\left(b_{\mathrm{bl}}-1\right)\right]} \tag{3}$$

In Eqs. 1–3, ω is the angular chopping frequency of radiation and σ and a are the complex thermal diffusion coefficient and the reciprocal of the thermal diffusion length ($a = 1/\mu$), respectively. Subscripts "p," "l," and "b" refer to the pyroelectric sensor, liquid sample, and backing material, respectively. The normalization of Eqs. 1 and 3 was performed with the signal obtained with the empty sensor, directly irradiated. The purpose of this normalization was to eliminate unknown experimental parameters such as the density of radiation, radiation to heat quantum efficiency, electrical time constant or the electronics, etc.

If, in addition, we imposed the condition of thermally very thick liquid layer (the distance sensor-backing is much larger than the thermal diffusion length in the liquid), $\exp(-\sigma_l L_l) = 0$, we obtain for the PPE signal:

$$V_{\infty}^{\mathrm{PPE}} = \frac{\sigma_p L_p}{\sigma_p L_p + b_{lp}} \tag{4}$$

If we normalize Eqs. 3 to 4, we get for the PPE signal

$$V_n^{\mathrm{PPE}} = \frac{\sigma_p L_p + b_{lp}}{(\sigma_p L_p) + b_{lp}\left[\frac{1-R_{bl}\exp(-2\sigma_l L_l)}{1+R_{bl}\exp(-2\sigma_l L_l)}\right]} \tag{5}$$

where $R_{ij} = (1 - b_{ij})/(b_{ij} + 1)$ represents the reflection coefficient of the thermal wave at the ij interface.

2.2 Photothermal Radiometry

If the irradiated material (sensor in our case) is optically opaque, the thermal radiation emittance of a material is given by

$$\delta W = 4\varepsilon\sigma_B T_0^3 \delta T \tag{6}$$

where ε is the sample's emissivity, σ_B is the Stephan–Boltzmann constant, T_0 is the steady-state temperature, and T is the sample's surface temperature [23].

Using the classical procedure, the fluctuations of the sample's surface temperature are given by [24]

$$\delta T = \frac{Q_0}{2k_p\sigma_p}\frac{1 + R_{lp}\exp(-2\sigma_p L_p)}{1 - R_{lp}\exp(-2\sigma_p L_p)} \tag{7}$$

where Q_0 is the absorbed radiant flux, R_1 from [24] is given in our particular case by

$$R_1 = -\gamma_{ap} = R_{ap} = \frac{1 - b_{ap}}{1 + b_{ap}} = 1 \text{ (a = air), and}$$

$$R_{lp} = \frac{1 - b_{lp} + R_{bl}(1 + b_{lp})\exp(-2\sigma_l L_l)}{1 + b_{lp} + R_{bl}(1 - b_{lp})\exp(-2\sigma_l L_l)}; \tag{8}$$

Combining Eqs. 6–8, we obtain for the PTR signal:

$$V^{\mathrm{PTR}} = K(f)\delta(f) = \frac{4K(f)\sigma_B T_0^3 \varepsilon Q_0}{2k_p\sigma_p}\frac{1 + R_{lp}\exp(-2\sigma_p L_p)}{1 - R_{lp}\exp(-2\sigma_p L_p)} \tag{9}$$

where $K(f)$ is an instrumental factor depending on the geometry of the system and electronic transfer function [25].

For a very thick liquid layer,

$$\exp(-2\sigma_l L_l) = 0 \quad \text{and} \quad R_{lp}^{\infty} = \frac{1 - b_{lp}}{1 + b_{lp}} \tag{10}$$

and the normalization signal becomes

$$V_{\infty}^{PTR} = \frac{4K(f)\sigma_B T_0^3 \varepsilon Q_0}{2k_p \sigma_p} \frac{1 + R_{lp}^{\infty} \exp(-2\sigma_p L_p)}{1 - R_{lp}^{\infty} \exp(-2\sigma_p L_p)} \tag{11}$$

Combining Eqs. 9–11, we get for the normalized PTR signal:

$$V_n^{PTR} = \frac{A_- B_+}{A_+ B_-} \tag{12}$$

where

$$\begin{aligned} A_{\pm} &= 1 + b_{lp} \pm (1 - b_{lp}) \exp(-2\sigma_p L_p) \\ B_{\pm} &= \left\{1 + b_{lp} + R_{bl}(1 - b_{lp}) \exp(-2\sigma_l L_l) \pm \left[1 - b_{lp} + R_{bl}(1 + b_{lp}) \exp(-2\sigma_l L_l)\right] \exp(-2\sigma_p L_p)\right\} \end{aligned} \tag{13}$$

We can conclude that both normalized FPPE and PTR signals (Eqs. 5 and 12–13) depend on the thermal diffusivity and effusivity of the pyroelectric sensor and liquid layer, respectively, and on the thermal effusivity of the backing material. Performing a thickness scan of the amplitude and/or phase of the FPPE and PTR signals (at constant chopping frequency), one can get information about one or, eventually two layers of the detection cell.

3 Mathematical Simulations

Mathematical simulations for the amplitude and phase of the FPPE and PTR signals are displayed in Figs. 2 and 3. The simulations were performed considering a 150 μm thick $LiTaO_3$ pyroelectric sensor ($e_p = 3.92 \times 10^3\ W \cdot s^{1/2} \cdot m^{-2} \cdot K^{-1}$; $\alpha_p = 1.56 \times 10^{-6}\ m^2 \cdot s^{-1}$), water ($e_l = 1.6 \times 10^3\ W \cdot s^{1/2} \cdot m^{-2} \cdot K^{-1}$; $\alpha_l = 14.6 \times 10^{-8}\ m^2 \cdot s^{-1}$) as liquid layer and 1 Hz chopping frequency. Four materials, with thermal effusivities ranging from $400\ W \cdot s^{1/2} \cdot m^{-2} \cdot K^{-1}$ to $35\,000\ W \cdot s^{1/2} \cdot m^{-2} \cdot K^{-1}$, were inserted as backing.

4 Conclusions

The theory developed in this article, together with the simulations from Figs. 2 and 3, indicates that, in all cases, for both FPPE and PTR signals, the information can be

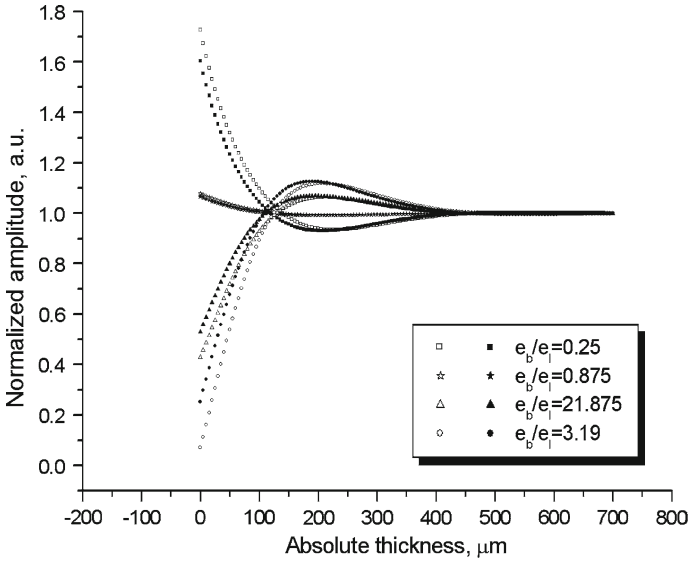

Fig. 2 Mathematical simulations of the behavior of the normalized amplitude of the FPPE (*empty symbols*) and PTR (*filled symbols*) signals as a function of coupling fluid's thickness (water) for different backing/coupling fluid effusivity ratios (pyroelectric sensor—150 μm thick, chopping frequency—1 Hz, $\mu_p/\mu_l = 10.68$)

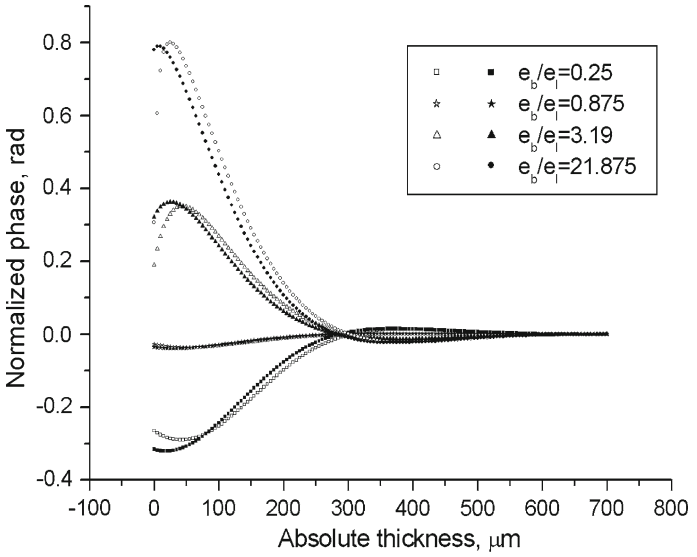

Fig. 3 Mathematical simulations of the behavior of the normalized phase of the FPPE (*empty symbols*) and PTR (*filled symbols*) signals as a function of coupling fluid's thickness (water) for different backing/coupling fluid effusivity ratios (pyroelectric sensor—150 μm thick, chopping frequency—1 Hz, $\mu_p/\mu_l = 10.68$)

extracted only from the thermally thin regime for the sensor and liquid layer. In the thermally thick regime for the sensor and/or liquid layer, both amplitude and phase saturate. The sensitivity of the methods depends on the effusivity ratio of the backing/liquid layer. For a given sensor ($LiTaO_3$ in our case), the thickness scan range is limited by the sensor's thickness and by the ratio (μ_p/μ_l) of the thermal diffusion lengths for the sensor and liquid layer [9,11,12].

The very similar behaviors of the FPPE and PTR signals give the opportunity to obtain information in *the same thickness range*; in conclusion, in one experimental run (one thickness scan), we can extract both FPPE and PTR information. The thermally thick regime for the coupling fluid, combined with the thermally thin regime for the sensor (the region of 500 μm to 700 μm from Figs. 2 and 3), is used for normalization purposes. Consequently, the normalization signal is contained in the same scanning run (no additional measurement is necessary). In the mean time this type of normalization eliminates unknown parameters such as infrared emissivity/absorptivity of the first layer (opaque sensor). On the other hand, the two methods preserve all the advantages of the TWRC technique. The most important (if compared with frequency scanning procedures) is the possibility of keeping a thermally thin regime for the sensor and changing the thermal regime of the liquid from thermally thin to thermally thick.

Stressing the predictions of the theory concerning the experimental procedure, the experimental parameters cannot be adjusted too much. For example, the best pyroelectric rigid sensors available on the market are $LiTaO_3$ single crystals of 100 μm to 500 μm thickness. In order to satisfy the thermally thin regime for the sensor, chopping frequencies lower than 50 Hz must be used. For typical coupling fluids presently used in the layered detection cells (based on water, ethylene glycol, various oils), the maximum thickness scanning range, including the thermally thin (giving the information) and thick (for normalization) regime for the liquid, is about 700 μm to 800 μm, respectively. Various values of the thermal diffusivity of the liquid layer combined with different chopping frequencies can influence to some extent this total scanning range and, at the same time, the range of the thermally thin regime for the liquid. Concerning the backing material, it can be a good or bad thermal conductor with a value of thermal effusivity ranging from $300\,W \cdot s^{1/2} \cdot m^{-2} \cdot K^{-1}$ to $400\,W \cdot s^{1/2} \cdot m^{-2} \cdot K^{-1}$ (wood, plastic—for example) up to $25\,000\,W \cdot s^{1/2} \cdot m^{-2} \cdot K^{-1}$ to $35\,000\,W \cdot s^{1/2} \cdot m^{-2} \cdot K^{-1}$ (aluminum, copper). The simulations from Figs. 2 and 3 indicate that the *sensitivity* of the method is high when the effusivity values of the backing and coupling fluid are different. However, contrary to this fact, the *accuracy* of the method in obtaining the thermal effusivity of the backing is higher when the effusivity of the liquid layer and backing material has close values (see, for example, Refs. [12,26]).

Overall, from a theoretical point of view, there are four independent sources of information (two amplitudes and two phases) and the obtained information refers to the thermal diffusivity or effusivity of the sensor and/or liquid layer, or the thermal effusivity of the backing material. Consequently, the two methods can offer complementary results if referring to different layers of the detection cell, or can reciprocally support each other, if referring to the same layer.

Study related to experimental investigations is in progress.

Acknowledgments This study was supported in part by the Romanian Ministry of Education and Research through the National Research Programs PN09 44 02 03 and PNII 372 and by Bilateral (NIRDIMT Cluj Napoca Univ. Littoral Dunkerque) Brancusi Project. One of the authors (D.D.) acknowledges the receipt of an Invited Professor Grant from Univ. Littoral Dunkerque, which greatly stimulated this study.

References

1. A. Mandelis, A. Matvienko, *Pyroelectric Materials and Sensors* (D. Remiens, Kerala, 2007), pp. 61–81
2. S. Delenclos, M. Chirtoc, A. Hadj Sahraoui, C. Kolinsky, J.M. Buisine, Rev. Sci. Instrum. **73**, 2773 (2002)
3. J. Shen, A. Mandelis, Rev. Sci. Instrum. **66**, 4999 (1995)
4. J. Shen, A. Mandelis, H. Tsai, Rev. Sci. Instrum. **69**, 197 (1998)
5. S. Pittois, M. Chirtoc, C. Glorieux, W. Bril, J. Thoen, Anal. Sci. (Jpn.) **17**, S110 (2001)
6. P.C. Menon, R.N. Rajesh, C. Glorieux, Rev. Sci. Instrum. **80**, 054904 (2009)
7. L.A. Balderas-Lopez, A. Mandelis, J.A. Garcia, Rev. Sci. Instrum. **71**, 2933 (2000)
8. L.A. Balderas-Lopez, A. Mandelis, Rev. Sci. Instrum. **74**, 700 (2003)
9. S. Delenclos, D. Dadarlat, N. Houriez, S. Longuemart, C. Kolinsky, A. Hadj Sahraoui, Rev. Sci. Instrum. **78**, 024902 (2007)
10. D. Dadarlat, C. Neamtu, R. Pop, M. Marinelli, F. Mercuri, J. Optoelectron. Adv. Mater. **9**, 2847 (2007)
11. M. Streza, M.N. Pop, K. Kovacs, V. Simon, S. Longuemart, D. Dadarlat, Laser Phys. **19**, 1340 (2009)
12. D. Dadarlat, M. Streza, M.N. Pop, V. Tosa, S. Delenclos, S. Longuemart, A. H. Sahraoui, J. Therm. Anal. Calorim. doi:10.1007/s10973-009-0513-6
13. D. Dadarlat, Laser Phys. **19**, 1330 (2009)
14. D. Dadarlat, C. Neamtu, Acta Chim. Slovenica **56**, 225 (2009)
15. M. Depriester, P. Hus, S. Delenclos, A.H. Sahraoui, Rev. Sci. Instrum. **76**, 074902 (2005)
16. M. Depriester, A.H. Sahraoui, P. Hus, F. Roussel, Appl. Phys. Lett. **94**, 231910 (2009)
17. F. Cernuski, A. Figari, J. Mater. Sci. **35**, 5891 (2000)
18. E. MacCormack, A. Mandelis, M. Munidasa, B. Farahbakhsh, H. Sang, Int. J. Thermophys. **18**, 221 (1997)
19. A. Gijsbertsen, D. Bicanic, J.L. Gielen, M. Chirtoc, Infrared Phys. Technol. **45**, 93 (2004)
20. U. Bernini, P. Maddalena, E. Massera, A. Ramaglia, Opt. Commun. **168**, 305 (1999)
21. A. Mandelis, M.M. Zver, J. Appl. Phys. **57**, 4421 (1985)
22. M. Chirtoc, G. Mihailescu, Phys. Rev. B **40**, 9606 (1989)
23. R. Santos, L.C.M. Miranda, J. Appl. Phys. **52**, 4194 (1981)
24. A. Mandelis, *Diffusion-Wave Fields: Mathematical Methods and Green Functions* (Springer, New York, 2006), pp. 148–151
25. J. Garcia, L. Nicolaides, P. Park, A. Mandelis, Anal. Sci. **17**, s89 (2001)
26. D. Dadarlat, M. Streza, M.N. Pop, V. Tosa, J. Phys. Conf. Ser. **182**, 012023 (2009)